SCIENCE CHINA
Earth Sciences

•RESEARCH PAPER•

October 2020 Vol.63 No.10: 1622–1632
https://doi.org/10.1007/s11430-019-9649-1

A multiple-proxy stalagmite record reveals historical deforestation in central Shandong, northern China

Liangcheng TAN[1,2,3,4*], Wen LIU[5,6,7], Tianli WANG[1], Peng CHENG[1,2], Jingjie ZANG[1], Xiqian WANG[1], Le MA[1], Dong LI[8], Jianghu LAN[1,2], R. Lawrence EDWARDS[9,10], Hai CHENG[3,1,9], Hai XU[11], Li AI[1], Yongli GAO[12] & Yanjun CAI[3]

[1] *State Key Laboratory of Loess and Quaternary Geology, Institute of Earth Environment, Chinese Academy of Sciences, Xi'an 710061, China;*
[2] *Center for Excellence in Quaternary Science and Global Change, Chinese Academy of Sciences, Xi'an 710061, China;*
[3] *Institute of Global Environmental Change, Xi'an Jiaotong University, Xi'an 710049, China;*
[4] *Open Studio for Oceanic-Continental Climate and Environment Changes, Pilot National Laboratory for Marine Science and Technology, Qingdao 266061, China;*
[5] *801 Institute of Hydrogeology and Engineering Geology, Shandong Provincial Bureau of Geology & Mineral Resources, Jinan 250014, China;*
[6] *Shandong Provincial Geo-mineral Engineering Exploration Institute, Jinan 250014, China;*
[7] *Shandong Engineering Research Center for Environmental Protection and Remediation on Groundwater, Jinan 250014, China;*
[8] *Library of Chang'an University, Xi'an 710064, China;*
[9] *Department of Earth Sciences, University of Minnesota, Minneapolis MN 55455, USA;*
[10] *School of Geography, Nanjing Normal University, Nanjing 210097, China;*
[11] *Institute of Surface-Earth System Science, Tianjin University, Tianjin 300072, China;*
[12] *Department of Geological Sciences, University of Texas at San Antonio, San Antonio TX 78249, USA*

Received November 15, 2019; revised May 1, 2020; accepted June 23, 2020; published online August 13, 2020

Abstract Evaluating anthropogenic impacts on regional vegetation changes during historical time is not only important for a better understanding of the Anthropocene but also valuable in improving the vegetation-climate models. In this study, we analyzed stable isotopes ($\delta^{18}O$, $\delta^{13}C$) and trace elements (Mg/Ca, Sr/Ca) of a stalagmite from Huangchao Cave in central Shandong, northern China. ^{230}Th and AMS ^{14}C dating results indicate the stalagmite deposited during 174BC and AD1810, with a hiatus between AD638 and 1102. Broad similarities of the $\delta^{18}O$ and trace elements in the stalagmite suggest they are reliable precipitation indexes. The $\delta^{13}C$ of the stalagmite, a proxy of vegetation change, was generally consistent with local precipitation and temperature variations on a centennial-scale before the 15th century. It typically varied from –9.6‰ to –6.3‰, indicating climate controlled C3 type vegetation during this period. However, a persistent and marked increasing trend in the $\delta^{13}C$ record was observed since the 15th century, resulting in $\delta^{13}C$ values from –7.7‰ to –1.6‰ in the next four centuries. This unprecedented $\delta^{13}C$ change caused by vegetation deterioration cannot be explained by climate change but is fairly consistent with the dramatically increasing population and farmland in Shandong. We suggest that the increasing deforestation and reclamation in central Shandong began to affect vegetation in the mountain region of central Shandong since the 15th century and severely destroyed or even cleared the forest during the 16th–18th century.

Keywords Speleothem, Stable isotopes, Trace elements, Deforestation, Human activity, 16th century

Citation: Tan L, Liu W, Wang T, Cheng P, Zang J, Wang X, Ma L, Li D, Lan J, Edwards R L, Cheng H, Xu H, Ai L, Gao Y, Cai Y. 2020. A multiple-proxy stalagmite record reveals historical deforestation in central Shandong, northern China. Science China Earth Sciences, 63: 1622–1632, https://doi.org/10.1007/s11430-019-9649-1

* Corresponding author (email: tanlch@ieecas.cn)

1. Introduction

The influence of human activities upon the Earth environment can be traced to the Pleistocene. These impacts become overwhelming during the Holocene (Dong et al., 2020), and brought mankind to a new epoch, the Anthropocene (Crutzen and Stoermer, 2000; Lewis and Maslin, 2015; Subramanian, 2019; Wang et al., 2019). Deforestation significantly altered the natural environment, accompanying the appearance of agriculture and herding in the early Holocene (Kaplan et al., 2009; Lewis and Maslin, 2015). Extensive deforestation caused soil erosion (Klimek et al., 2006; Vanacker et al., 2003), disturbed the ecosystem and element cycles (Kassa et al., 2017; Sahani and Behera, 2001), as well as affected water balance (Coe et al., 2009; Kaplan et al., 2009; Lean and Warrilow, 1989; Nogherotto et al., 2013). It is noted that changes in water balance were not limited to local areas where deforestation occurred but expanded to a wider region by atmospheric circulation (Boers et al., 2017; Coe et al., 2009; Durieux et al., 2003; Potter et al., 1975; Sen et al., 2004; Spracklen and Garcia-Carreras, 2015). In addition, deforestation also influenced the land surface and air temperature (Davin and Noblet-Ducoudré, 2010; Lee et al., 2011; Li et al., 2016; Winckler et al., 2019), although these effects are still not clearly understood (Lejeune et al., 2018). A better understanding of historical deforestation will help estimate the biogeographical effects of land use on climate and contribute to the improvement of climate models.

Human activities have long existed in Shandong province, China. Various cultures flourished there during the Neolithic Age, such as the Beixin, Dawenkou and Longshan culture systems. As early as in Dawenkou culture (4300–2200BC), settled agriculture was developed in central Shandong, with millet as the main crop. Longshan culture (2100–1900BC) was a Chalcolithic culture, and after that, this region entered the Bronze Age (Zhang, 2006). During historical time, Shandong became one of the most important economic and cultural centers of China. Grains produced in Shandong were transported along the Yellow River, supplying the central plain. Frequently and intensively human activities strongly influenced the local ecosystem. Shen Kuo (AD1031–1095), an ancient scientist, recorded in his book "*Brush Talks from Dream Brook*" that "The pine forests between Qi and Lu regions (Qi and Lu were ancient kingdoms in Shandong) were totally destroyed" (Shen, 2009). However, historical records were discontinuous and only provided very limited and short time intervals of the deforestation history. It remains ambiguous when and to what extent human activities strongly affected the vegetation in mountain areas of Shandong. As a result, it is important to reveal vegetation information from various geological records for a better understanding of the deforestation history in this region.

Stalagmite is one kind of secondary carbonate which is deposited in caves. Because it is highly-resolved, continuously-deposited, accurately-dated, and contains multiple proxies, it becomes an ideal terrestrial archive for Quaternary climate and environment reconstruction (Cheng et al., 2019; Fairchild and Treble, 2009; McDermott, 2004). By using stalagmite oxygen isotopic ($\delta^{18}O$) records, scientists have reconstructed accurately-dated Asian monsoon history over the past several glacial-interglacial cycles (Cai et al., 2015; Cheng et al., 2009, 2016; Wang et al., 2001, 2008; Yuan et al., 2004) and revealed monsoon climate patterns and dynamics on different timescales (Cai et al., 2010; Hu et al., 2008; Jiang et al., 2016; Li et al., 2019a; Li et al., 2007; Liu D B et al., 2015; Tan et al., 2018a, 2019; Yang et al., 2019; Yang et al., 2010; Zhang et al., 2008; Zhao et al., 2010). The carbon isotope ($\delta^{13}C$) is another important geochemical proxy in stalagmite. It can record past vegetation changes (vegetation types and density) overlying the cave, although hydroclimate conditions can also influence its variation on a short timescale (Breitenbach et al., 2019; Columbu et al., 2019; Luo et al., 2013; McDermott, 2004; Shen et al., 2016; Yasur et al., 2019). For example, Dorale et al. (1998) found that the vegetation in Missouri, USA varied between forests, savannas, and prairies during 75–55 ka by using the $\delta^{13}C$ records of four stalagmites from this region. Denniston et al. (2000) further studied the Holocene vegetation dynamics in the Ozark Highlands, USA by using stalagmite $\delta^{13}C$ records. Moreover, deforestation history can be recorded in speleothem $\delta^{13}C$. Zhang et al. (2015) suggested that the persistent and massive deforestation associated with large-scale immigration caused a prominent enrichment in the stalagmite $\delta^{13}C$ values from Shennonggong Cave in northern Jiangxi, China since AD700. The abnormally positive shift of the stalagmite $\delta^{13}C$ from Zhijin Cave in the past 300 years (Kuo et al., 2011) was also ascribed to the destruction of local forest by the immigration to western Guizhou, China.

Recently, Wang et al. (2015) reported a 1000-year stalagmite (KY1) record from Kaiyuan Cave in central Shandong and examined anthropogenic influences on local vegetation since the 14th century. However, was the anthropogenic influence local or regional? Had human activities significantly affected the vegetation in the first millennium? They are still unclear. In this paper, we studied a multiple proxy ($\delta^{18}O$, $\delta^{13}C$, Mg/Ca and Sr/Ca) stalagmite (HC2) from Huangchao Cave, 105 km north of Kaiyuan Cave and reconstructed regional climate and vegetation changes spanning the past 2200 years. Together, with the KY1 and historical records, we evaluated anthropogenic deforestation and vegetation deterioration in the history of central Shandong.

2. Study area, cave and sample

Huangchao Cave (118°20′E, 36°37′N, 518 m a.s.l., meter above sea level) is located in Qingzhou, central Shandong of China (Figure 1). The local semi-humid climate is strongly controlled by East Asian monsoon, with an annual mean precipitation of 690 mm and annual mean temperature of 12.5°C (data from Yiyuan station, 50 km southwest of the Huangchao Cave). More than 70% of the rainfall occurred during summer monsoon seasons (June to September). During winter, the winter monsoon and westerly jet maintain cold and dry conditions in this region.

Huangchao Cave is horizontally developed in fractures of the Ordovician limestone and dolomite bedrocks of Xuanyang Mountain, with 4–10 m ceiling rock. The cave, with a small entrance, is about 170 m in length. Only one passage was developed, with its width of 1.0–8.2 m, and height of 1.2–9.3 m (Figure 2). Various kinds of speleothems, including soda straws, stalactites, stalagmites, flowstones were observed in the cave. The cave is 180–340 m higher than local groundwater level during different seasons. As a result, atmospheric precipitation is the only supply of drip water. A lot of graffiti and charcoal were observed in the cave, indicating frequent human activities during historical times. There is an abandoned temple, and many other structure remains above the cave (Figure 3). Today, the vegetation overlying the cave is composed of grass, undershrub and secondary forest (Figure 3).

A 5.5 cm long calcite stalagmite, HC2, was collected in the middle part of the passage in 2017. The stalagmite displayed clear laminas when halved and polished (Figure 4). A hiatus was observed between 2.7 and 2.75 cm from the top. Below the hiatus, the stalagmite was composed by yellowish-brown, compact calcite. It was dark grey above the hiatus, containing an abundance of charcoal.

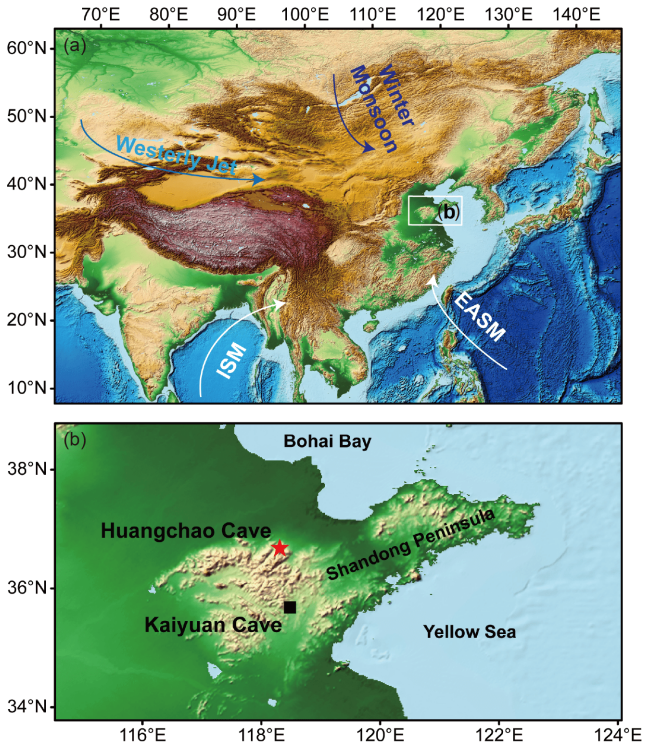

Figure 1 Location of Huangchao Cave. (a) Overview map showing the study region. (b) Enlarged regional topographic map showing the location of Huangchao Cave and Kaiyuan Cave in central Shandong, China. Topographic GTOPO30 data from the USGS EROS Center (Earth Resources Observation and Science Center: http://eros.usgs.gov/#/Find_Data/Products_and_Data_Available/gtopo30_info). The arrows in Panel (a) denote the direction of the East Asian Summer Monsoon (EASM), Indian Summer Monsoon (ISM), winter monsoon and westerly jet which influence the climate of China.

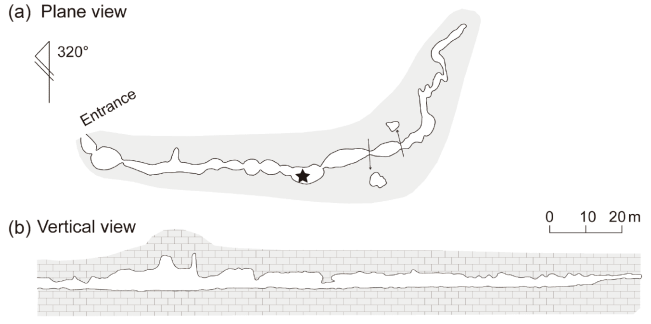

Figure 2 (a) Plane view and (b) cross section of Huangchao Cave. The black star indicates where the stalagmite HC2 was collected in 2017.

3. Methods

3.1 U-Th and AMS^{14}C dating

Eleven powder subsamples, each about 50 mg, were collected with a hand-held carbide dental drill, paralleling the growth planes of the stalagmite. The chemical procedure used to separate uranium and thorium followed those described by (Edwards et al., 1987). Measurements were performed on a multi-collector inductively coupled plasma mass spectrometer (ICP-MS) in Xi'an Jiaotong University, China by using the U-Th dating method (Cheng et al., 2013).

Because there is an abundance of charcoal in the upper part of the stalagmite, we also collected 6 pieces of charcoal subsamples for AMS^{14}C age measurement. The charcoal samples were released by 1N HCl from the carbonate subsamples, then rinsed repeatedly until neutral and oven-dried overnight at 60°C. Pretreated samples and CuO powders were placed into 9-mm quartz tubes, evacuated to $<10^{-5}$ Torr, (1 Torr=1.33322×10^2 Pa) and then combusted. The CO_2 was converted catalytically to graphite using the zinc method, where CO_2 is reduced by Zn powder in the presence of an Fe catalyst (Jull, 2007; Slota et al., 1987). The ^{14}C content of the graphite was measured in the Xi'an AMS center, with a measurement uncertainty of ^{14}C/^{12}C for a modern sample of better than 0.2% in routine operation (Zhou et al., 2007;

Figure 3 Photos showing the landscape of Huangchao Cave in winter. (a) Secondary forest, undershrub and grass overlying Huangchao Cave. The abandoned temple is also shown. (b) Historical structure remains in the cave area. (c) The stone monument recording the rebuilding of the temple in AD1585. (d) The entrance of Huangchao Cave. (e) A chamber inside the cave, with abundant charcoal and graffiti on the wall and floor. (f) Sampling of the stalagmite HC2.

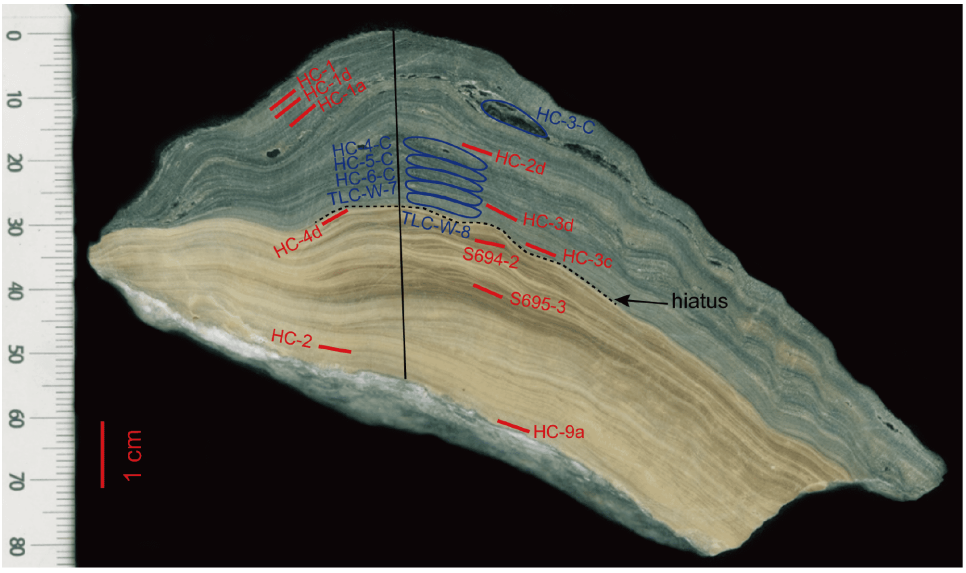

Figure 4 Polished section of HC2. A hiatus occurred between 2.7 and 2.75 cm from the top. The black line along the growth axis of the stalagmite indicates the sampling paths of stable isotopes and trace elements. The locations of the ^{230}Th and AMS^{14}C dating subsamples are also shown.

Zhou et al., 2006).

3.2 Isotopic and elemental analyses

Subsamples for stable isotope analyses were drilled out along the growth axis of the stalagmite at intervals of 0.5 mm. A total of 111 stable isotopic measurements were performed on a Finnigan MAT-252 mass spectrometer equipped with a Kiel III Carbonate Device at the IEECAS. We added one national standard GBW04405 (also referred as TTB1, with the δ^{18}O of –8.49±0.14‰ and δ^{13}C of 0.57 ±0.03‰) every 15 samples for the control. The replicates showed that the precision of δ^{18}O and δ^{13}C analyses are better than 0.1‰ (2σ, VPDB). We also drilled 55 sub-

samples, every 1 mm along the growth axis, for elemental (Mg, Sr, Ca) analyses. The 1–2 mg powders were dissolved in 2 mL HNO_3 (1 mol L^{-1}), and measured on an Agilent 5100 Inductively Coupled Plasma Optical Emission Spectrometry (ICP-OES) at the IEECAS (Li et al., 2019b). We add one in-house standard, N1, every five subsamples, and the precision of Mg/Ca and Sr/Ca ratios are about 1% (1σ).

4. Results

The U-Th dating results are shown in Table 1. It indicates the U concentrations of HC2 range from 339 to 534 ppb (1 ppb=1 ng g^{-1}). The Th concentrations in the lower part of HC2 (below 2.75 cm) vary from 1.2 to 3.6 ppb. However, they are more than ten times higher in the upper part, except for the topmost part of the stalagmite (Table 1). As a result, the dating errors of the ^{230}Th ages of the upper part are very large and not reliable. In contrast, the AMS^{14}C dating provides reliable ages for this part because of abundant charcoal (Table 2). We then apply the Monte-Carlo simulation and COPRA methods (Breitenbach et al., 2012) to establish the age model of HC2 (Figure 5). The results suggest that HC2 grew from 174BC to AD1810 with a hiatus occurring between AD638 and 1102.

The isotope and element data are shown in Figure 6. The δ^{18}O values of the stalagmite vary from –9.2‰ to –7.3‰, with significantly centennial- to decadal-scale fluctuations during the past 2200 years (Figure 6d). Comparing with δ^{18}O, there are large fluctuation amplitudes in the δ^{13}C series, varying from –9.6‰ to –1.6‰ (Figure 6a). The δ^{13}C values are lighter than –6‰ before the 16th century, and heavier than –6‰ after AD1500, reaching –1.6‰ in the 18th century. Most notably, a persistent increasing trend was observed since the 15th century in the δ^{13}C series. The Mg/Ca (Figure 6b) and Sr/Ca (Figure 6c) records of HC2 show similar patterns and are in general consistent with the δ^{18}O variations.

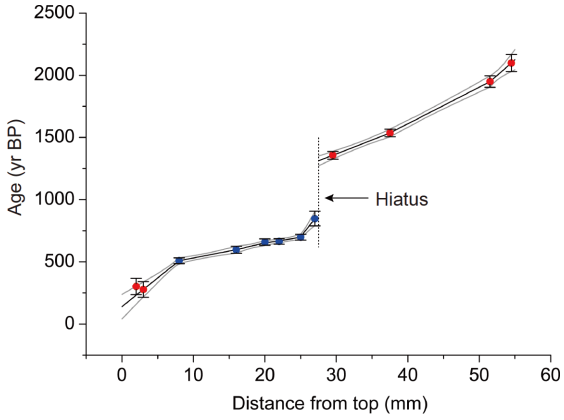

Figure 5 Age-depth model of HC2. Age models were established using 2000 Monte-Carlo simulations (Breitenbach et al., 2012). Grey lines represent the 95% confidence interval and the black line is the median age. Error bars are 2σ error. The red and blue dots are ^{230}Th and calibrated AMS ^{14}C dates, respectively. The dotted line shows that a hiatus occurred between AD638 and AD1102. The medium ages of the top two ^{230}Th dates are reversed, but consistent within dating errors. Here we included the second one in the age model.

5. Discussion

5.1 δ^{18}O and trace elements recorded historical climate change in central Shandong

The δ^{18}O record of HC2 well replicates the KY1 record (Figure 6f) from Kaiyuan Cave (Wang et al., 2015) during

Table 1 ^{230}Th dating results of HC2[a)]

Sample No.	Depth (mm)	^{238}U (ppb)	^{232}Th (ppt)	^{230}Th/^{232}Th (atomic×10^{-6})	δ^{234}U* (measured)	^{230}Th/^{238}U (activity)	^{230}Th age (yr) (uncorrected)	^{230}Th age (yr) (corrected)	$\delta^{234}U_{Initial}$** (corrected)	^{230}Th age (yr BP)& (corrected)
HC-1	2	534.1±29.8	3572±72	23±1	1233.2±34.6	0.0093±0.0006	457±28	370±66	1234±35	303±66
HC-1d	3	347.0±0.4	2320±47	23±1	1397.4±2.7	0.0093±0.0006	425±26	344±63	1399±3	277±63
HC-1a	**5**	**395.9±0.5**	**46932±941**	**13±0**	**1436.5±3.0**	**0.0966±0.0008**	**4394±39**	**2978±1004**	**1449±5**	**2911±1004**
HC-2d	**13**	**423.3±0.6**	**11445±229**	**68±1**	**1325.1±2.6**	**0.1119±0.0006**	**5356±28**	**5020±239**	**1344±3**	**4953±239**
HC-3d	**25**	**339.1±0.5**	**20790±417**	**18±0**	**1547.3±3.2**	**0.0682±0.0007**	**2952±32**	**2252±496**	**1557±4**	**2185±496**
HC-3c	**26.5**	**376.1±0.6**	**23045±462**	**34±1**	**1484.5±3.0**	**0.1265±0.0005**	**5672±25**	**4959±506**	**1505±4**	**4892±506**
HC-4d	**28**	**342.0±0.3**	**10426±209**	**42±1**	**1485.9±2.1**	**0.0779±0.0006**	**3461±28**	**3106±253**	**1499±2**	**3039±253**
S694-2	29.5	355.8±0.5	1238±26	164±4	1600.1±2.9	0.0347±0.0004	1463±16	1424±32	1607±3	1357±32
S695-3	37.5	388.4±0.6	1387±28	183±4	1649.4±2.8	0.0397±0.0003	1642±14	1603±31	1657±3	1536±31
HC-2	51.5	427.0±0.9	2320±47	143±3	1496.3±3.4	0.0472±0.0003	2079±14	2016±47	1505±3	1949±47
HC-9a	54.5	453.4±0.6	3018±61	125±3	1469.3±3.2	0.0504±0.0009	2244±41	2165±69	1478±3	2098±69

a) The error is 2σ error. The dates in bold are excluded from the age model. 1 ppt=1 ng L^{-1}. decay constants: λ_{238}=1.55125×10^{-10} (Jaffey et al., 1971) and λ_{234}=2.82206×10^{-6} (Cheng et al., 2013). Th decay constant: λ_{230}=9.1705×10^{-6} (Cheng et al., 2013). *$\delta^{234}U=((^{234}U/^{238}U)_{activity}-1)\times1000$. **$\delta^{234}U_{initial}$ was calculated based on ^{230}Th age (T), i.e., $\delta^{234}U_{initial}=\delta^{234}U_{measured}\times e^{\lambda 234\times T}$. Corrected ^{230}Th ages assume the initial ^{230}Th/^{232}Th atomic ratio of 4.4±2.2×10^{-6}. Those are the values for a material at secular equilibrium, with the bulk earth ^{232}Th/^{238}U value of 3.8. The errors are arbitrarily assumed to be 50%. B.P. stands for "Before Present" where the "Present" is defined as the year AD1950

Table 2 AMS^{14}C dating results of HC2

Lab No.	Sample No.	Depth from top (mm)	Dated material	^{14}C age		^{14}C calibrated age (cal yr BP) (1σ)		
				Age (yr BP)	Error	Upper	Lower	Median probability
XA19330	HC-3-C	8	Charcoal	449	23	501	516	509
XA19331	HC-4-C	16	Charcoal	563	28	537	627	598
XA19332	HC-5-C	20	Charcoal	685	25	572	672	659
XA19333	HC-6-C	22	Charcoal	694	22	656	673	664
XA18196	TLC-W-7	25	Charcoal	775	24	678	725	698
XA18197	TLC-W-8	27	Charcoal	908	25	787	904	848

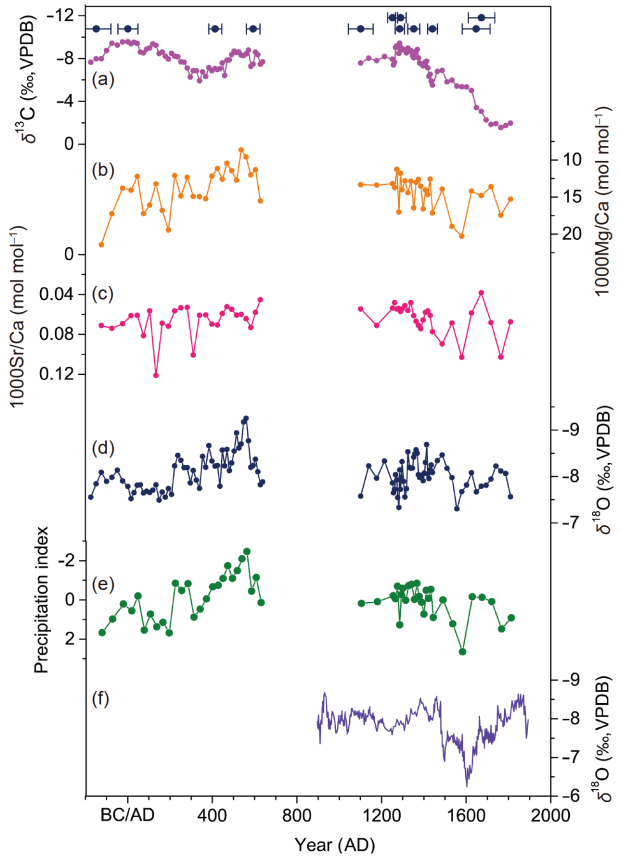

Figure 6 Stable isotope and trace element records of HC2 from Huangchao Cave. (a) δ^{13}C record, (b) Mg/Ca record, (c) Sr/Ca record, (d) δ^{18}O record, (e) PCA1 of δ^{18}O, Mg/Ca and Sr/Ca records as regional precipitation index record, with more negative values indicating more rainfall. (f) Stalagmite δ^{18}O record from Kaiyuan Cave (Wang et al., 2015), 105 km south of Huangchao Cave. The blue dots with errors in panel A show the dating points.

the overlapping time period (AD1100–1810). The "replication test" indicates HC2 was deposited under equilibrium fractionation condition (Dorale et al., 1998; Tan et al., 2019; Wang et al., 2001). Previous studies suggest that stalagmite δ^{18}O from monsoonal China under equilibrium fractionations could be influenced by variations of large-scale atmospheric circulation (i.e. monsoon intensity), moisture sources, upstream rainout, and/or regional rainfall amount (Cai et al., 2010; Cheng et al., 2016; Hu et al., 2008; Liu J B et al., 2015; Liu et al., 2014; Maher and Thompson, 2012; Tan et al., 2011, 2018a, 2018b; Wang et al., 2001; Yuan et al., 2004; Zhang et al., 2008). When comparing the speleothem δ^{18}O with instrumental records, as well as historical and other hydrological records, scientists suggested a negative relationship between stalagmite δ^{18}O and rainfall amount in the northern monsoonal China on centennial- to decadal- and annual-timescales (Li et al., 2017; Tan et al., 2014, 2011; Zhang et al., 2008). Model simulations also support this negative stalagmite δ^{18}O-rainfall amount relationship in northern China (Liu et al., 2014). Following previous findings, we interpret our HC2 δ^{18}O variations as dominated by local precipitation changes.

Mg^{2+} and Sr^{2+} in speleothems come from the soil and bedrock overlying the cave and are mainly controlled by karst-water processes (Fairchild and Treble, 2009). Prolonged water-rock interaction during drier conditions can cause prior calcite precipitation (PCP) in the slower flow and enhance the Mg^{2+} and Sr^{2+} concentrations in speleothems due to preferential removal of Ca^{2+} (Arienzo et al., 2019; Carolin et al., 2019; Fairchild et al., 2000; Fairchild and Treble, 2009; Goede et al., 1998; Li et al., 2005). In addition, a drier climate would favor closed system conditions in the karst aquifer, causing enrichment in Mg and Sr via a longer water-rock interaction. The opposite occurs during wetter conditions (Fairchild and Treble, 2009; Griffiths et al., 2016; Zhang et al., 2018). The significant positive correlation between the HC2 δ^{18}O and Mg/Ca (r=0.46, p<0.01) further confirms the inverse stalagmite δ^{18}O/rainfall amount relationship in central Shandong.

We then applied the principal components analysis (PCA) method to the δ^{18}O, Mg/Ca and Sr/Ca records of the stalagmite (Figure 6e). The PCA 1 explains 53% of the total variance, indicating that it can represent common variations of the three series, i.e. precipitation variations. Therefore, we regard it as a precipitation index for central Shandong, with negative values indicating more rainfall and positive values indicating less rainfall. The average resolution of the newly developed precipitation record is about 25 years. Our record (Table S1) suggests that precipitation decreased in central Shandong during the 2nd century compared with the previous 200 years. From the 3rd century, the precipitation

gradually increased, with the wettest period occurring in the middle 6th century, followed by a decline in the next few decades. Because of the deposition hiatus of the stalagmite, we cannot obtain climate information during AD640–1100. The climate in central Shandong during the 12th–15th century was relatively wet, with a drought occurring in the late 13th century. From the 16th century, the precipitation began to decrease, with the driest period occurring in the late 16th century. After the driest period, the precipitation increased. It declined again in the late 18th century.

5.2 δ^{13}C recorded historical vegetation changes in central Shandong

The carbon isotope in stalagmite mainly comes from dissolved inorganic carbon in drip water and may be influenced by isotopic fractionation during the carbonate deposition. There are three sources of carbon in cave drip water. One is the atmospheric CO_2, and the other two are carbonate bedrock and biogenic soil CO_2 (Li et al., 1997; McDermott, 2004; Tan et al., 2013). However, the δ^{13}C values of the atmospheric CO_2 before the Industry Revolution in the 18th century are relatively constant on centennial- to decadal-scale, about –6.4‰ (Craig and Keeling, 1963; Francey et al., 1999). The typical δ^{13}C value of bedrock is about 1‰, which has little influence on the δ^{13}C of drip water under open cave systems. Under closed cave system, slow (fast) seepage water during dry (wet) condition could increase (decrease) the time of water-rock interaction, and dissolve more (less) carbonate bedrock, enhancing (reducing) the δ^{13}C in stalagmite (Li et al., 1997). Most natural cave systems are partly open, and the changes of δ^{13}C in stalagmite are mainly influenced by the third source, dissolved CO_2 from plant root's respiration and soil organic matter's decomposition, which is controlled by the vegetation type and density above the cave (Baldini et al., 2005; Breitenbach et al., 2019; Dorale et al., 1998; Genty et al., 2003; McDermott, 2004; Pérez-Mejías et al., 2019; Springer et al., 2010; Yasur et al., 2019). If the overlying vegetation is C3 plants, like the forest, the stalagmite δ^{13}C values would typically fall in the range of –14‰ to –6‰ under the carbon equilibrium fractionation condition. In contrast, they would typically fall in the range of –6‰ to 2‰ if the overlying vegetation is C4 plants (Cerling et al., 1989; McDermott, 2004). On the other hand, reduced vegetation cover can decrease the plant root's respiration and soil organic content, decrease the soil biogenic CO_2, resulting in heavier δ^{13}C values in drip water and speleothems (Breitenbach et al., 2019; Columbu et al., 2019; Kennett et al., 2012; McDermott, 2004; Pérez-Mejías et al., 2019). In both cases, dry climate would reduce C3 vegetation development and cause more positive δ^{13}C in speleothems than that during wet climate conditions. Besides, drier climate increases seepage water residence time, favors bedrock dissolution, degassing and PCP in the unsaturated zone, which can also enhance the δ^{13}C values in speleothem (Baker et al., 1997; Luo et al., 2013; Oster et al., 2012; Shen et al., 2016). In this case, the δ^{13}C should positively correlate with trace element variations.

On a centennial scale, the δ^{13}C changes, typically between –9.6‰ and –6.3‰, in our stalagmite were generally consistent with the temperature (Figure 7b, Ge et al., 2013) and local precipitation variations (Figure 7a) before the 15th century, with warmer/wetter (cold/dry) climate corresponding to more (less) negative δ^{13}C. The coherence suggests C3 dominated vegetation, which was controlled by climate change during this period. However, the in-phase δ^{13}C-climate relationship was broken after AD1400. Since then, a prominently positive shift was observed in the stalagmite δ^{13}C record, with its values increasing from –7.7‰ to –1.6‰ in the next four centuries, and never returning to –6‰ after AD1500. Similar variations were also recorded in the KY1 δ^{13}C values (Wang et al., 2015) (Figure 7d). The consistent

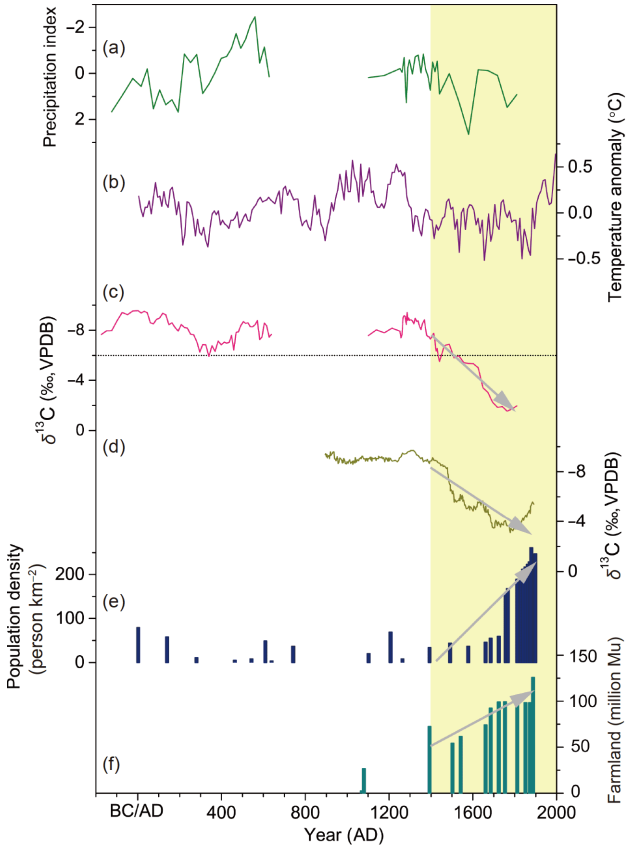

Figure 7 Comparisons of stalagmite δ^{13}C records from central Shandong with climate and human activity records during historical times. (a) Precipitation record in central Shandong deduced from HC2. (b) Temperature anomaly of China (Ge et al., 2013). (c) δ^{13}C record of HC2 from Huangchao Cave. (d) δ^{13}C record of KY1 from Kaiyuan Cave (Wang et al., 2015). (e) Population density in Shandong during historical times (Liang, 2018; Lu and Teng, 2000). (f) Farmland area (1 Mu=667 m^2) record in Shandong during historical times (Liang, 2018). Dashed line in panel C represents the δ^{13}C value of –6‰. Grey arrows denote the increasing trends of speleothem δ^{13}C, population density and farmland area since the 15th century.

variations of the two stalagmite records, distributed in the north and south part of central Shandong mountains, suggest a persistent reduction of C3 type vegetation in this region since the 15th century. The vegetation deterioration was so severe that it might change from the C3 dominated plant assemblages to the C4 dominated plants after AD1500. This unprecedented, prominent vegetation change cannot be explained by climate change. Precipitation variations revealed by proxies from our stalagmite and KY1 (Wang et al., 2015) did not show a similar declining trend during this period (Figure 6). At the same time, the average temperature from the 16th to 18th centuries did not change much either (Figure 7b) (Ge et al., 2013). Most importantly, the cold climate during the Little Ice Age (AD1400–1850) was unfavorable for natural C4 vegetation's development (Cerling et al., 1989) in semi-humid Shandong. Even today, the natural vegetation in central Shandong is not dominated by C4 plants. Therefore, the only driving force for the marked vegetation deterioration since the 15th century could be the increasing deforestation and reclamation in central Shandong caused by abundant human activities.

5.3 Anthropogenic deforestation in central Shandong during historical times

The anthropogenic deforestation in Shandong was recorded in *The Book of Songs* (*Shijing*), which collected poems from the 11th century BC to 6th century BC. A poem named "*Bi Palace*" in the chapter of "*Lu Hymns*" collected in *The Book of Songs* recorded:

Culai Mountain's pines are tall and flourish (徂徠之松),

Xinfu Mountain's cypresses are strong and lush (新甫之柏).

They can be used as pillars and rafters (是断是度),

They can be measured by rulers (是寻是尺).

The Culai and Xinfu mountains are located in central Shandong. As a result, this is the earliest literature recording anthropogenic deforestation in Shandong. However, considering the coherent variations of the stalagmite $\delta^{13}C$ and climate (Figure 7), the magnitude and extent of deforestation were limited and did not significantly change the vegetation in the mountain region of central Shandong before the 15th century. With the prosperous society and increasing population during the Ming (AD1368–1644) and Qing dynasties (AD1644–1911), more and more mountain areas were reclaimed (Liang, 2018; Wang, 1994). It was recorded that the reclamation area of Shandong was the 3rd largest over the country in AD1396 (Li, 1987). The persistent increase of $\delta^{13}C$ in the stalagmites from Huangchao Cave and Kaiyuan Cave since the 15th century correlated well with the increasing trend of population and farmland in Shandong (Liang, 2018; Lu and Teng, 2000) (Figure 7), suggesting increasing deforestation and reclamation in this region. Indeed, foxtail (*Setaria italica*) and common millet (*Panicum miliaceum*), which are C4 crops, had long been cultivated in northern China during historical and prehistorical times (Yang and Li, 2015). No later than AD1603, another important C4 crop, maize (*Zea mays Linn.*), was also introduced to Shandong (Wang, 2006). The $\delta^{13}C$ of stalagmites from both caves are well above –6‰ after the beginning of the 16th century, suggesting that extensive human activities already seriously destroyed or even cleared the forest in this region.

Abundant human activities in this region during historical times are also evidenced from structure remains inside and outside Huangchao Cave (Figure 3). The cave is named after a rebel leader, Huang Chao (AD820–884), whose army rose against the Tang Dynasty (AD618–907). According to local legend, his army hid in the cave and kept fighting against the Tang government after Huang Chao's death in AD884. We still can see the steps cut in the flowstone of the cave chamber, which is said to be a meeting room for the army (ECQS, 1989). The age of the abandoned temple (Figure 3a) is not known. However, the stone monument (Figure 3c) recorded the temple was rebuilt in AD1585 (Yiyou Year (the traditional Chinese calendar, every 60 year as a cycle) during the Emperor Wanli (AD1563–1620) in Ming Dynasty). In addition, the abundance of charcoal (Figure 3e) deposited on the floor and walls of the cave, as well as in the stalagmite, were evidence of wood burning. All the evidence confirms enhanced deforestation in this region since the 15th century.

6. Conclusions

Multiple geochemical proxies ($\delta^{18}O$, $\delta^{13}C$, Mg/Ca, Sr/Ca) of a stalagmite from Huangchao Cave reveal the climate and vegetation changes in central Shandong, China over the past 2200 years, except for the hiatus between AD640 and 1100. The results suggest a typical C3 dominated vegetation in the mountain region of central Shandong before the 15th century. Vegetation change during this period was mainly controlled by climate change, despite some anthropogenic deforestation. However, increasing deforestation and reclamation caused by massive human activities began to destroy the vegetation in the mountain region of central Shandong since the 15th century, and may have cleared the forest from the 16th to 18th century.

Acknowledgements *We thank the two anonymous reviewers for their constructive suggestions. This work was supported by the National Natural Science Foundation of China (Grant No. 41991252), the Strategic Priority Research Program (Grant No. XDB40000000), the International Partnership Program (Grant No. 132B61KYSB20170005) of Chinese Academy of Sciences, and the National Natural Science Foundation of China (Grant No. 41888101). It was also partly supported by the USA National Science Foundation (Grant Nos. 0908792, 1211299 & 1702816 to R. Lawrence*

EDWARDS and Hai CHENG), the 111 Program of China (Grant No. D19002) and the Belt & Road Center for Climate and Environment Studies of IEECAS.

References

Arienzo M M, Mehterian S, Swart P K, Broad K, Kakuk B. 2019. Drip-water and calcite geochemistry variations in a monitored Bahamas cave. Geochem Geophys Geosyst, 20: 4306–4318

Baker A, Ito E, Smart P L, McEwan R F. 1997. Elevated and variable values of ^{13}C in speleothems in a British cave system. Chem Geol, 136: 263–270

Baldini J U L, McDermott F, Baker A, Baldini L M, Mattey D P, Railsback L B. 2005. Biomass effects on stalagmite growth and isotope ratios: A 20th century analogue from Wiltshire, England. Earth Planet Sci Lett, 240: 486–494

Boers N, Marwan N, Barbosa H M J, Kurths J. 2017. A deforestation-induced tipping point for the South American monsoon system. Sci Rep, 7: 41489

Breitenbach S F M, Rehfeld K, Goswami B, Baldini J U L, Ridley H E, Kennett D J, Prufer K M, Aquino V V, Asmerom Y, Polyak V J, Cheng H, Kurths J, Marwan N. 2012. Constructing proxy records from age models (COPRA). Clim Past, 8: 1765–1779

Breitenbach S F M, Plessen B, Waltgenbach S, Tjallingii R, Leonhardt J, Jochum K P, Meyer H, Goswami B, Marwan N, Scholz D. 2019. Holocene interaction of maritime and continental climate in Central Europe: New speleothem evidence from Central Germany. Glob Planet Change, 176: 144–161

Cai Y J, Fung I Y, Edwards R L, An Z S, Cheng H, Lee J E, Tan L C, Shen C C, Wang X F, Day J A, Zhou W J, Kelly M J, Chiang J C H. 2015. Variability of stalagmite-inferred Indian monsoon precipitation over the past 252,000 y. Proc Natl Acad Sci USA, 112: 2954–2959

Cai Y J, Tan L C, Cheng H, An Z S, Edwards R L, Kelly M J, Kong X G, Wang X F. 2010. The variation of summer monsoon precipitation in central China since the last deglaciation. Earth Planet Sci Lett, 291: 21–31

Carolin S A, Walker R T, Day C C, Ersek V, Sloan R A, Dee M W, Talebian M, Henderson G M. 2019. Precise timing of abrupt increase in dust activity in the Middle East coincident with 4.2 ka social change. Proc Natl Acad Sci USA, 116: 67–72

Cerling T E, Quade J, Wang Y, Bowman J R. 1989. Carbon isotopes in soils and palaeosols as ecology and palaeoecology indicators. Nature, 341: 138–139

Cheng H, Edwards R L, Broecker W S, Denton G H, Kong X, Wang Y, Zhang R, Wang X. 2009. Ice age terminations. Science, 326: 248–252

Cheng H, Edwards R L, Sinha A, Spötl C, Yi L, Chen S, Kelly M, Kathayat G, Wang X, Li X, Kong X, Wang Y, Ning Y, Zhang H. 2016. The Asian monsoon over the past 640000 years and ice age terminations. Nature, 534: 640–646

Cheng H, Lawrence Edwards R, Shen C C, Polyak V J, Asmerom Y, Woodhead J, Hellstrom J, Wang Y, Kong X, Spötl C, Wang X, Calvin Alexander Jr E. 2013. Improvements in ^{230}Th dating, ^{230}Th and ^{234}U half-life values, and U-Th isotopic measurements by multi-collector inductively coupled plasma mass spectrometry. Earth Planet Sci Lett, 371-372: 82–91

Cheng H, Zhang H, Zhao J, Li H, Ning Y, Kathayat G. 2019. Chinese stalagmite paleoclimate researches: A review and perspective. Sci China Earth Sci, 62: 1489–1513

Coe M T, Costa M H, Soares-Filho B S. 2009. The influence of historical and potential future deforestation on the stream flow of the Amazon River—Land surface processes and atmospheric feedbacks. J Hydrol, 369: 165–174

Columbu A, Spötl C, De Waele J, Yu T L, Shen C C, Gázquez F. 2019. A long record of MIS 7 and MIS 5 climate and environment from a western Mediterranean speleothem (SW Sardinia, Italy). Quat Sci Rev, 220: 230–243

Craig H, Keeling C D. 1963. The effects of atmospheric NO_2 on the measured isotopic composition of atmospheric CO_2. Geochim Cosmochim Acta, 27: 549–551

Crutzen P J, Stoermer E F. 2000. The Anthropocene. IGBP Newsletter, 41: 17–18

Davin E L, de Noblet-Ducoudré N. 2010. Climatic impact of global-scale deforestation: Radiative versus nonradiative processes. J Clim, 23: 97–112

Denniston R F, González L A, Asmerom Y, Reagan M K, Recelli-Snyder H. 2000. Speleothem carbon isotopic records of Holocene environments in the Ozark Highlands, USA. Quat Int, 67: 21–27

Dong G H, Li R, Lu M X, Zhang D J, James N. 2020. Evolution of human-environmental interactions in China from the Late Paleolithic to the Bronze Age. Prog Phys Geogr-Earth Environ, 44: 233–250

Dorale J A, Edwards R L, Ito E, Gonzalez L A. 1998. Climate and Vegetation History of the Midcontinent from 75 to 25 ka: A Speleothem Record from Crevice Cave, Missouri, USA. Science, 282: 1871–1874

Durieux L, Machado L A T, Laurent H. 2003. The impact of deforestation on cloud cover over the Amazon arc of deforestation. Remote Sens Environ, 86: 132–140

Editorial Committee of Qingzhou Shizhi (ECQS). 1989. History of Qingzhou (in Chinese). Tianjin: Nankai University Press

Edwards R L, Chen J H, Wasserburg G J. 1987. ^{238}U-^{234}U-^{230}Th-^{232}Th systematics and the precise measurement of time over the past 500000 years. Earth Planet Sci Lett, 81: 175–192

Fairchild I J, Borsato A, Tooth A F, Frisia S, Hawkesworth C J, Huang Y, McDermott F, Spiro B. 2000. Controls on trace element (Sr-Mg) compositions of carbonate cave waters: Implications for speleothem climatic records. Chem Geol, 166: 255–269

Fairchild I J, Treble P C. 2009. Trace elements in speleothems as recorders of environmental change. Quat Sci Rev, 28: 449–468

Francey R J, Allison C E, Etheridge D M, Trudinger C M, Enting I G, Leuenberger M, Langenfelds R L, Michel E, Steele L P. 1999. A 1000-year high precision record of δ^{13}C in atmospheric CO_2. Tellus B-Chem Phys Meteorol, 51: 170–193

Ge Q S, Hao Z X, Zheng J Y, Shao X M. 2013. Temperature changes over the past 2000 yr in China and comparison with the Northern Hemisphere. Clim Past, 9: 1153–1160

Genty D, Blamart D, Ouahdi R, Gilmour M, Baker A, Jouzel J, Van-Exter S. 2003. Precise dating of Dansgaard-Oeschger climate oscillations in western Europe from stalagmite data. Nature, 421: 833–837

Goede A, McCulloch M, McDermott F, Hawkesworth C. 1998. Aeolian contribution to strontium and strontium isotope variations in a Tasmanian speleothem. Chem Geol, 149: 37–50

Griffiths M L, Kimbrough A K, Gagan M K, Drysdale R N, Cole J E, Johnson K R, Zhao J X, Cook B I, Hellstrom J C, Hantoro W S. 2016. Western Pacific hydroclimate linked to global climate variability over the past two millennia. Nat Commun, 7: 11719

Hu C Y, Henderson G M, Huang J H, Xie S C, Sun Y, Johnson K R. 2008. Quantification of Holocene Asian monsoon rainfall from spatially separated cave records. Earth Planet Sci Lett, 266: 221–232

Jaffey A H, Flynn K F, Glendenin L E, Bentley W C, Essling A M. 1971. Precision measurement of half-lives and specific activities of ^{235}U and ^{238}U. Phys Rev C, 4: 1889–1906

Jiang X Y, Wang X Y, He Y Q, Hu H M, Li Z Z, Spötl C, Shen C C. 2016. Precisely dated multidecadally resolved Asian summer monsoon dynamics 113.5–86.6 thousand years ago. Quat Sci Rev, 143: 1–12

Jull A. 2007. Radiocarbon dating AMS method. Encycl Quat Sci, 2911–2918

Kaplan J O, Krumhardt K M, Zimmermann N. 2009. The prehistoric and preindustrial deforestation of Europe. Quat Sci Rev, 28: 3016–3034

Kennett D J, Breitenbach S F M, Aquino V V, Asmerom Y, Awe J, Baldini J U L, Bartlein P, Culleton B J, Ebert C, Jazwa C, Macri M J, Marwan N, Polyak V, Prufer K M, Ridley H E, Sodemann H, Winterhalder B, Haug G H. 2012. Development and disintegration of Maya political systems in response to climate change. Science, 338: 788–791

Klimek K, Lanczont M, Nogaj-Chachaj J. 2006. Historical deforestation as

a cause of alluviation in small valleys, subcarpathian loess plateau, Poland. Reg Environ Change, 6: 52–61
Kuo T S, Liu Z Q, Li H C, Wan N J, Shen C C, Ku T L. 2011. Climate and environmental changes during the past millennium in central western Guizhou, China as recorded by Stalagmite ZJD-21. J Asian Earth Sci, 40: 1111–1120
Lean J, Warrilow D A. 1989. Simulation of the regional climatic impact of Amazon deforestation. Nature, 342: 411–413
Lee X, Goulden M L, Hollinger D Y, Barr A, Black T A, Bohrer G, Bracho R, Drake B, Goldstein A, Gu L, Katul G, Kolb T, Law B E, Margolis H, Meyers T, Monson R, Munger W, Oren R, Paw U K T, Richardson A D, Schmid H P, Staebler R, Wofsy S, Zhao L. 2011. Observed increase in local cooling effect of deforestation at higher latitudes. Nature, 479: 384–387
Lejeune Q, Davin E L, Gudmundsson L, Winckler J, Seneviratne S I. 2018. Historical deforestation locally increased the intensity of hot days in northern mid-latitudes. Nat Clim Change, 8: 386–390
Lewis S L, Maslin M A. 2015. Defining the Anthropocene. Nature, 519: 171–180
Li D, Tan L, Cai Y, Jiang X, Ma L, Cheng H, Edwards R L, Zhang H, Gao Y, An Z. 2019a. Is Chinese stalagmite $\delta^{18}O$ solely controlled by the Indian summer monsoon? Clim Dyn, 53: 2969–2983
Li D, Tan L, Guo F, Cai Y, Sun Y, Xue G, Cheng X, Yan H, Cheng H, Edwards R L, Gao Y, Kelley J. 2019b. Application of Avaatech X-ray fluorescence core-scanning in Sr/Ca analysis of speleothems. Sci China Earth Sci, 62: 964–973
Li H C, Ku T L, Stott L D, Yuan D X, Chen W J, Li T Y. 1997. Interannual-resolution $\delta^{13}C$ record of stalagmites as proxy for the changes in precipitation and atmospheric CO_2 in Shihua Cave, Beijing (in Chinese with English abstract). Carsol Sin, 16: 285–295
Li H C, Ku T L, You C F, Cheng H, Edwards R L, Ma Z B, Tsai W, Li M D. 2005. $^{87}Sr/^{86}Sr$ and Sr/Ca in speleothems for paleoclimate reconstruction in Central China between 70 and 280 kyr ago. Geochim Cosmochim Acta, 69: 3933–3947
Li J H. 1987. Historical dynamics of the forest in Shandong (in Chinese). Agric Archaeol, (1): 219–225
Li T Y, Yuan D X, Li H C, Yang Y, Wang J L, Wang X Y, Li J Y, Qin J M, Zhang M L, Lin Y S. 2007. High-resolution climate variability of southwest China during 57–70 ka reflected in a stalagmite $\delta^{18}O$ record from Xinya Cave. Sci China Ser D-Earth Sci, 50: 1202–1208
Li X L, Cheng H, Tan L C, Ban F M, Sinha A, Duan W H, Li H Y, Zhang H W, Ning Y F, Kathayat G. 2017. The East Asian summer monsoon variability over the last 145 years inferred from the Shihua Cave record, North China. Sci Rep, 7: 7078
Li Y, Zhao M S, Mildrexler D J, Motesharrei S, Mu Q, Kalnay E, Zhao F, Li S C, Wang K C. 2016. Potential and actual impacts of deforestation and afforestation on land surface temperature. J Geophys Res-Atmos, 121: 14372
Liang F Z. 2018. Households, Farmland and Land Tax During Chinese Historical Time (in Chinese). Beijing: China Publishing House
Liu D B, Wang Y J, Cheng H, Edwards R L, Kong X G. 2015. Cyclic changes of Asian monsoon intensity during the early mid-Holocene from annually-laminated stalagmites, central China. Quat Sci Rev, 121: 1–10
Liu J B, Chen J H, Zhang X J, Li Y, Rao Z G, Chen F H. 2015. Holocene East Asian summer monsoon records in northern China and their inconsistency with Chinese stalagmite $\delta^{18}O$ records. Earth-Sci Rev, 148: 194–208
Liu Z Y, Wen X Y, Brady E C, Otto-Bliesner B, Yu G, Lu H Y, Cheng H, Wang Y J, Zheng W P, Ding Y H. 2014. Chinese cave records and the East Asia summer monsoon. Quat Sci Rev, 83: 115–128
Lu Y, Teng Z Z. 2000. General History of Chinese Population (in Chinese). Jinan: Shandong People's Publishing
Luo W J, Wang S J, Xie X N, Zhou Y C, Li T Y. 2013. Stable carbon isotope variations in cave percolation waters and their implications in four caves of Guizhou, China. Acta Geol Sin-Engl Ed, 87: 1396–1411
Maher B A, Thompson R. 2012. Oxygen isotopes from Chinese caves: Records not of monsoon rainfall but of circulation regime. J Quat Sci, 27: 615–624
McDermott F. 2004. Palaeo-climate reconstruction from stable isotope variations in speleothems: A review. Quat Sci Rev, 23: 901–918
Nogherotto R, Coppola E, Giorgi F, Mariotti L. 2013. Impact of Congo Basin deforestation on the African monsoon. Atmos Sci Lett, 14: 45–51
Oster J L, Montañez I P, Kelley N P. 2012. Response of a modern cave system to large seasonal precipitation variability. Geochim Cosmochim Acta, 91: 92–108
Pérez-Mejías C, Moreno A, Sancho C, Martín-García R, Spötl C, Cacho I, Cheng H, Edwards R L. 2019. Orbital-to-millennial scale climate variability during Marine Isotope Stages 5 to 3 in northeast Iberia. Quat Sci Rev, 224: 105946
Potter G L, Ellsaesser H W, MacCracken M C, Luther F M. 1975. Possible climatic impact of tropical deforestation. Nature, 258: 697–698
Sen O L, Wang Y, Wang B. 2004. Impact of Indochina deforestation on the East Asian Summer Monsoon. J Clim, 17: 1366–1380
Shen K. 2009. Brush Talks From Dream Brook (in Chinese). Beijing: China Publishing House
Shen W, Wang J L, Wang J L, Jiang X S, Mao Q Y. 2016. Hydrochemistry and $\delta^{13}C_{DIC}$ features of cave water in Naduo cave, Guizhou and their influencing factors (in Chinese with English abstract). Carsol Sin, 35: 98–105
Slota Jr P J, Jull A J T, Linick T W, Toolin L J. 1987. Preparation of small samples for ^{14}C accelerator targets by catalytic reduction of CO. Radiocarbon, 29: 303–306
Spracklen D V, Garcia-Carreras L. 2015. The impact of Amazonian deforestation on Amazon basin rainfall. Geophys Res Lett, 42: 9546–9552
Springer G S, White D M, Rowe H D, Hardt B, Nivanthi Mihimdukulasooriya L, Cheng H, Edwards R L. 2010. Multiproxy evidence from caves of Native Americans altering the overlying landscape during the late Holocene of east-central North America. Holocene, 20: 275–283
Subramanian M. 2019. Anthropocene now: Influential panel votes to recognize Earth's new epoch. Nature, doi: 10.1038/d41586-019-01641-5
Tan L C, An Z S, Huh C A, Cai Y J, Shen C C, Shiau L J, Yan L, Cheng H, Edwards R L. 2014. Cyclic precipitation variation on the western Loess Plateau of China during the past four centuries. Sci Rep, 4: 6381
Tan L C, Cai Y J, An Z S, Edwards R L, Cheng H, Shen C C, Zhang H W. 2011. Centennial- to decadal-scale monsoon precipitation variability in the semi-humid region, northern China during the last 1860 years: Records from stalagmites in Huangye Cave. Holocene, 21: 287–296
Tan L C, Cai Y J, Cheng H, Edwards R L, Gao Y L, Xu H, Zhang H W, An Z S. 2018a. Centennial- to decadal-scale monsoon precipitation variations in the upper Hanjiang River region, China over the past 6650 years. Earth Planet Sci Lett, 482: 580–590
Tan L C, Cai Y J, Cheng H, Edwards R L, Lan J H, Zhang H W, Li D, Ma L, Zhao P P, Gao Y L. 2018b. High resolution monsoon precipitation changes on southeastern Tibetan Plateau over the past 2300 years. Quat Sci Rev, 195: 122–132
Tan L C, Shen C C, Löwemark L, Chawchai S, Edwards R L, Cai Y J, Breitenbach S F M, Cheng H, Chou Y C, Duerrast H, Partin J W, Cai W J, Chabangborn A, Gao Y L, Kwiecien O, Wu C C, Shi Z G, Hsu H H, Wohlfarth B. 2019. Rainfall variations in central Indo-Pacific over the past 2700 y. Proc Natl Acad Sci USA, 116: 17201–17206
Tan L C, Zhang H W, Qin S J, An Z S. 2013. Climatic and Anthropogenic Impacts on $\delta^{13}C$ Variations in a Stalagmite from Central China. Terr Atmos Ocean Sci, 24: 333–343
Vanacker V, Vanderschaeghe M, Govers G, Willems E, Poesen J, Deckers J, De Bievre B. 2003. Linking hydrological, infinite slope stability and land-use change models through GIS for assessing the impact of deforestation on slope stability in high Andean watersheds. Geomorphology, 52: 299–315
Wang B Q. 2006. Studies on changes of cropping structure and their influences in Shandong since Ming and Qing dynasties (in Chinese). Dissertation for Doctoral Degree. Nanjing: Nanjing Agricultural Uni-

versity
Wang Q, Zhou H Y, Chi H, Cheng K, Wang H Y, Ma Q Q, Wang C S. 2015. The stalagmite records of climate and environment change on the western Shandong peninsula during the past 1000 years: δ^{18}O and δ^{13}C values (I) (in Chinese with English abstract). Mar Geol Quat Geol, 35: 135–142
Wang T L, Tan L C, Xu H, Zang J J, Li D, Lan J H, Han Y M, Li L. 2019. The selection of a primary marker for the Anthropocene. Sci Bull, 64: 1643–1645
Wang Y J, Cheng H, Edwards R L, An Z S, Wu J Y, Shen C C, Dorale J A. 2001. A high-resolution absolute-dated late Pleistocene monsoon record from Hulu Cave, China. Science, 294: 2345–2348
Wang Y J, Cheng H, Edwards R L, Kong X G, Shao X H, Chen S T, Wu J Y, Jiang X Y, Wang X F, An Z S. 2008. Millennial- and orbital-scale changes in the East Asian monsoon over the past 224,000 years. Nature, 451: 1090–1093
Wang Z T, Sheng L X. 1994. China Ecological Environment Change and Population Pressure (in Chinese). Beijing: China Environmental Science Press
Winckler J, Lejeune Q, Reick C H, Pongratz J. 2019. Nonlocal effects dominate the global mean surface temperature response to the biogeophysical effects of deforestation. Geophys Res Lett, 46: 745–755
Yang Q, Li X Q. 2015. Investigation of the controlled factors influencing carbon isotope composition of foxtail and common millet on the Chinese Loess Plateau. Sci China Earth Sci, 58: 2296–2308
Yang X L, Yang H, Wang B Y, Huang L J, Shen C C, Edwards R L, Cheng H. 2019. Early-Holocene monsoon instability and climatic optimum recorded by Chinese stalagmites. Holocene, 29: 1059–1067
Yang Y, Yuan D X, Cheng H, Zhang M L, Qin J M, Lin Y S, Zhu X Y, Edwards R L. 2010. Precise dating of abrupt shifts in the Asian monsoon during the last deglaciation based on stalagmite data from Yamen Cave, Guizhou Province, China. Sci China Earth Sci, 53: 633–641
Yasur G, Ayalon A, Matthews A, Zilberman T, Marder O, Barzilai O, Boaretto E, Hershkovitz I, Bar-Matthews M. 2019. Climatic and environmental conditions in the Western Galilee, during Late Middle and Upper Paleolithic periods, based on speleothems from Manot Cave, Israel. J Human Evol, doi: 10.1016/j.jhevol.2019.04.004
Yuan D X, Cheng H, Edwards R L, Dykoski C A, Kelly M J, Zhang M L, Qing J M, Lin Y S, Wang Y J, Wu J Y, Dorale J A, An Z S, Cai Y J. 2004. Timing, duration, and transitions of the last Interglacial Asian monsoon. Science, 304: 575–578
Zhang H W, Cai Y J, Tan L C, Cheng H, Qin S J, An Z S, Edwards R L, Ma L. 2015. Large variations of δ^{13}C values in stalagmites from southeastern China during historical times: Implications for anthropogenic deforestation. Boreas, 44: 511–525
Zhang H B, Griffiths M L, Chiang J C H, Kong W W, Wu S T, Atwood A, Huang J H, Cheng H, Ning Y F, Xie S C. 2018. East Asian hydroclimate modulated by the position of the westerlies during Termination I. Science, 362: 580–583
Zhang P Z, Cheng H, Edwards R L, Chen F H, Wang Y J, Yang X L, Liu J, Tan M, Wang X F, Liu J H, An C L, Dai Z B, Zhou J, Zhang D Z, Jia J H, Jin L Y, Johnson K R. 2008. A test of climate, sun, and culture relationships from an 1810-year Chinese cave record. Science, 322: 940–942
Zhang Z H. 2006. Introduction to Chinese Archaeology (in Chinese). Nanjing: Nanjing University Press
Zhao K, Wang Y J, Edwards R L, Cheng H, Liu D B. 2010. High-resolution stalagmite δ^{18}O records of Asian monsoon changes in central and southern China spanning the MIS 3/2 transition. Earth Planet Sci Lett, 298: 191–198
Zhou W J, Lu X F, Wu Z K, Zhao W N, Huang C H, Li L L, Chen P, Xin Z H. 2007. New results on Xi'an-AMS and sample preparation systems at Xi'an-AMS center. Nucl Instrum Meth B, 262: 135–142
Zhou W J, Zhao X L, Lu X F, Liu L, Wu Z K, Cheng P, Zhao W N, Huang C H. 2006. The 3MV multi-element AMS in Xi'an, China: Unique features and preliminary tests. Radiocarbon, 48: 285–293

(Responsible editor: Xiaoqiang LI)